# Experimental ($^{13}$C NMR) and Theoretical (*ab Initio* Molecular Orbital Calculations) Studies on the Prototropic Tautomerism of Benzotriazole and Some Derivatives Symmetrically Substituted on the Benzene Ring

**Jarosław Poznański,*,†,‡ Andżelika Najda,† Maria Bretner,† and David Shugar*,†,§**

*Institute of Biochemistry and Biophysics, Polish Academy of Sciences, 5a Pawińskiego St. 02-106 Warszawa, Poland, Institute of Physical Chemistry, Polish Academy of Sciences, Kasprzaka 44/52, 01-224 Warszawa, Poland, and Division of Biophysics, Institute of Experimental Physics, University of Warsaw, 93 Żwirki i Wigury St., 02-089 Warszawa, Poland*

*Received: February 27, 2007; In Final Form: May 16, 2007*

The prototropic tautomerism in anhydrous DMSO of benzotriazole and six derivatives symmetrically substituted on the benzene ring (5,6-dichloro, tetrachloro, 4,7-dibromo, tetrabromo, 5,6-dimethyl, and tetramethyl), was followed by both experimental ($^{13}$C NMR and UV spectroscopy) and theoretical methods. In all of the analyzed systems, predominance of the asymmetric form, N(1)/N(3) protonated, was found. The rates of the N(1)−H ↔ N(3)−H prototropic equilibrium, estimated by $^{13}$C NMR techniques, were in the medium exchange regime of 300−3000 $s^{-1}$, and are correlated with the spectroscopically determined p$K_a$ values in aqueous medium, and the anionic forms are the putative rate-limiting intermediate states.

## I. Introduction

The prototropic tautomerism of benzotriazole (**1**, BT) has long attracted considerable attention,[1] more recently because of its widespread use as a scaffold for the synthesis of an enormous number of analogues with potential antimetabolic activities,[2,3] one example of which is presented in detail below.

BT may exist in three tautomeric forms (Scheme 1), two of which, the N(1)−H and the N(3)−H, are degenerate in the absence of isotope labeling or of asymmetric substitution on the benzene ring.

Both the asymmetric N(1)−H and symmetric N(2)−H forms of BT have been reported to exist in the gas phase, but the data concerning their relative populations are contradictory. Thus, UV spectroscopy at 30−90 °C indicated that the N(2)−H tautomer is enthalpically favored by ∼4 kcal $mol^{-1}$,[4,5] but FTIR spectroscopy in the temperature range 110−230 °C indicated that the N(1)−H tautomer is stabilized by ∼1 kcal $mol^{-1}$.[6] Recent theoretical calculations estimate the energy difference between tautomers in the gas phase as low as 0.31 kcal/mol.[7]

X-ray diffraction[8] and IR and Raman spectroscopy[9] of crystals of BT showed it to exist as the asymmetric N(1)/N(3)−H form, while $^{14}$N NMR spectroscopy on the amorphous solid,[10] and IR spectroscopy in a KBr matrix[11] pointed to strong predominance of this form.

The stability of the N(1)−H form is known to be increased in a polar environment, and predominates in BT−water binary clusters,[12] as well as in aqueous,[13] $CO_2$/acetone,[14,15] benzene,[15] and isooctane[13] solutions.

The mechanism of proton transfer between tautomers is less well-known, although for azoles it has been proposed that it proceeds, even between adjacent nitrogen atoms, as a process

**SCHEME 1**

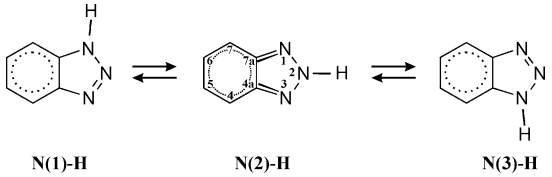


more complex than simple solvent-stabilized ionization.[1] Despite this, for solutions of unsubstituted triazoles in TMF, the lack of kinetic dependence on solute concentration, and negative entropy of the barrier, pointed to intramolecular proton transfer.[16] Kinetics of proton transfer in BT, performed with the aid of $^1$H NMR spectroscopy in anhydrous THF,[17] and with the aid of $^{15}$N NMR spectroscopy in acetone solution,[14] indicated a barrier to prototropy of ∼11 kcal/mol.

The protomeric equilibrium of BT derivatives interacting with biomolecules is less well-known. There are, however, two examples of a BT derivative carrying an exchangeable proton, TBBT, bound to two different proteins, recorded in the Protein Data Bank. One is the complex with the α-subunit of *Zea mays* CK2 kinase (1J91).[18] The other is the complex with *Homo sapiens* phospho-CDK2/cyclin A (1P5E).[19] The two proteins display relatively high sequence homology and almost identical spatial organization of the catalytic centers. TBBT binds to identical regions of the enzymes, but in a different manner.[19] The tautomeric forms of the bound TBBT, deduced from the bond-length distribution, differ. In the 1P5E structure, TBBT is bound in the symmetric N2−H form, whereas in 1J91 it is in the asymmetric, N1−H form. Comparison of both complexes is presented in Supporting Information.

Insofar as we are aware, there have been no reports on the prototropic equilibrium, and the kinetics of proton transfer, for benzotriazoles with a substituted benzene ring, the subject of the present communication. Our interest in the foregoing stemmed from the finding[20] that some benzotriazole derivatives, in which the benzene ring is halogenated, were found to be

* Corresponding authors. E-mail: jarek@ibb.waw.pl (J.P.); shugar@ibb.waw.pl (D.S.).
† Institute of Biochemistry and Biophysics, Polish Academy of Sciences.
‡ Institute of Physical Chemistry, Polish Academy of Sciences.
§ Division of Biophysics, Institute of Experimental Physics, University of Warsaw.

10.1021/jp071611h CCC: $37.00 
Published on Web 06/22/2007

**SCHEME 2**

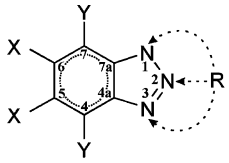


| Id | acronym | compound | X | Y | R | Ref. |
|---|---|---|---|---|---|---|
| 1 | BT | benzotriazole | H | H | H | |
| 2 | DBBT | 4,7-dibromobenzotriazole | H | Br | H | 23 |
| 3 | DCBT | 5,6-dichlorobenzotriazole | Cl | H | H | 24 |
| 4 | DMBT | 5,6-dimethylbenzotriazole | $CH_3$ | H | H | 24 |
| 5 | TBBT | 4,5,6,7-tetrabromobenzotriazole | Br | Br | H | 25 |
| 6 | TCBT | 4,5,6,7-tetrachlorobenzotriazole | Cl | Cl | H | 25 |
| 7 | TMBT | 4,5,6,7-tetramethylbenzotriazole | $CH_3$ | $CH_3$ | H | 22 |
| 8 | m$^1$TBBT | $N^1$-methyl-4,5,6,7-tetrabromobenzotriazole | Br | Br | $CH_3$ - N(1) | 23, 24 |
| 9 | m$^2$TBBT | $N^2$-methyl-4,5,6,7-tetrabromobenzotriazole | Br | Br | $CH_3$ - N(2) | 23, 24 |
| 10 | pr$^1$DMBT | $N^1$-propyl-5,6-dimethylbenzotriazole | $CH_3$ | H | $C_3H_7$ - N(1) | this work |
| 11 | pr$^2$DMBT | $N^2$-propyl-5,6-dimethylbenzotriazole | $CH_3$ | H | $C_3H_7$ - N(2) | this work |
| 12 | BT-rib | $N^1$-β-D-ribofuranose-benzotriazole | H | H | ribose - N(1) | 23 |
| 13 | DBBT-rib | $N^1$-β-D-ribofuranose-4,7-dibromobenzotriazole | H | Br | ribose - N(1) | 23 |
| 14 | DCBT-rib | $N^1$-β-D-ribofuranose-5,6-dichlorobenzotriazole | Cl | H | ribose - N(1) | 23 |
| 15 | TMBT-rib | $N^1$-β-D-ribofuranose-4,5,6,7-tetramethylbenzotriazole | $CH_3$ | $CH_3$ | ribose - N(1) | 23 |
| 16 | PMBT | $N^1$,4,5,6,7-pentamethylbenzotriazole | $CH_3$ | $CH_3$ | $CH_3$ - N(1) | *in silico* |

selective competitive inhibitors of the ubiquitous protein kinase CK2 (formerly known as casein kinase 2). The most potent of these, 4,5,6,7-tetrabromobenzotriazole (TBBT) is quite selective for this kinase relative to more than 30 other kinases.[21] The corresponding 4,5,6,7-tetrachlorobenzotriazole (TCBT) is a poorer inhibitor.[22] In ongoing efforts to elucidate the mode of binding of these analogues, and to develop more potent and selective inhibitors, it is obviously desirable to determine the prototropic tautomerism of those compounds, as well as the effects of substituents on dissociation of the triazole proton.

## II. Material and Methods

Benzotriazole (**1**) and 1-iodopropane were products of Aldrich (USA), and 1,8-Diazaobicyclo[5.4.0]undec-7-ene (DBU) was from Fluka.

High grade deuterated $d_6$-DMSO was from Armar Chemicals (015200.0010) and, to avoid uptake of water from the atmosphere, was taken from the ampule immediately prior to addition to the sample for NMR measurements.

The various derivatives of BT employed in this study, and their abbreviations, are shown in Scheme 2. The syntheses of two of these, **10** and **11,** hitherto not reported, are described below.

**Chemical Syntheses.** Melting points (uncorrected) were determined in open capillary tubes using a Büchi apparatus B504. Analytical thin-layer chromatography (TLC) was on Merck 0.2 mm silica gel 60 $F_{254}$ plates. Preparative separations were conducted on Merck 2 mm silica gel 60 $F_{254}$ plates. Mass spectra were recorded on a Micromass ESI Q-TOF.

**pr$^1$DMBT (10) and pr$^2$DMBT (11).** To a solution of **4** (310 mg, 2 mmol) in dioxane (17 mL) and DBU (1.15 mL) was added 1-iodopropane (718 $\mu$L, 7 mmol), and the solution was heated at 50 °C for 12 h. The reaction mixture was filtered, brought to dryness, the residue dissolved in diethyl ether, and extracted with water. The ether layer was brought to small volume and products isolated on preparative silica gel plates (*n*-hexane: acetone 20:1.5). Elution with acetone and evaporation gave the following. (a) 169 mg (yield 42%) of pr$^1$DMBT (**10**), mp 65−

65.5 °C. MS for $C_{11}H_{16}N_3$ MS ($ES^+$): found, 190.457; calculated, 190.268. $^1$H NMR (DMSO-$d_6$): $\delta$ 0.83 (t, 3, 3′-$CH_3$), 1.90 (dt, 2, 2′-$CH_2$), 2.36 (s, 3, 5-$CH_3$), 2.39 (s, 3, 6-$CH_3$), 4.59 (t, 2, 1′-$CH_2$), 7.64 (s, 1, 7-H), 7.76 (s, 1, 4-H). $^{13}$C NMR (DMSO-$d_6$): $\delta$ 11.1 (3′-$CH_3$), 19.9 (5-$CH_3$), 20.5 (6-$CH_3$), 22.8 (2′-$CH_2$), 48.9 (1′-$CH_2$), 109.8 (C(7)), 118.1 (C(4)), 132.0 (C(7a)), 133.4 (C(5)), 137.2 (C(6)), 144.5 (C(4a)). (b) 112 mg (yield 28%) pr$^2$DMBT (**11**), mp 81−82 °C. MS for $C_{11}H_{16}N_3$ MS ($ES^+$): found, 190.099; calculated, 190.268. $^1$H NMR (DMSO-$d_6$): $\delta$ 0.84 (t, 3, 3′-$CH_3$), 2.00 (dt, 2, 2′-$CH_2$), 2.35 (s, 6, 5-$CH_3$ and 6-$CH_3$), 4.62 (t, 2, 1′-$CH_2$), 7.64 (s, 2, 4-H and 7-H). $^{13}$C NMR (DMSO-$d_6$): $\delta$ 10.8 (3′-$CH_3$), 20.2 (5-$CH_3$ and 6-$CH_3$), 22.8 (2′-$CH_2$), 57.0 (1′-$CH_2$), 116.0 (C(4) and C(7)), 136.1 (C(5) and C(6)), 142.9 (C(4a) and C(7a)).

**NMR Spectroscopy**. NMR spectra were recorded on a Varian Unity plus 500 MHz spectrometer at 298 K in DMSO for compound concentrations in the range ∼100 $\mu$M to 1 mM, depending on sample solubility. $^{13}$C spectra were recorded directly with broadband proton decoupling, using a spectral width of 200 ppm and 30K data points during acquisition. The $^{13}$C spectra of the more soluble N(1)-ribosyl derivatives of DBBT and DCBT were additionally recorded at ∼1 mM in aqueous medium.

Spectra were processed and analyzed with the aid of the MestRe−C (version 2.3a) program.[26] $^{13}$C spectra were transformed using 64K zero-filling following Lorenzian filtering resulting in 0.5−15 Hz resonance broadening, depending on the quality of the spectrum and estimated original resonance line width. Chemical shift values were relative to DMSO (septuplet centered at 39.43 ppm). Resonance line widths were estimated using the Lorenzian line shape fitting program, based on the Marquardt−Levenberg algorithm[27] implemented in the Gnuplot program.[28] The $^1$H spectra for identification of the structures of **10** and **11** were processed using a $\pi$/4 shifted squared sine−bell filter and 32K zero-filling prior to Fourier transformation, and referred to DMSO (quintuplet, 2.50 ppm).

Resonance assignments for the parent BT were adopted from Jagerovic et al.[14] $^{13}$C resonance assignments for BT derivatives were done with the aid of GIAO-derived NMR shielding parameters, and verified by comparison with published data for close structural analogues.[29,30]

**Spectrophotometric Titration.** This was performed with a Cary 3 UV−vis spectrophotometer, equipped with a thermostated (25 °C) cell holder. Measurements of pH in the range of 2−10 were carried out with an accuracy of ±0.05 using a CP315 m pH meter (Elmetron, Poland) equipped with a combination semimicro electrode (Orion, U.K.) and temperature sensor. The 220−320 nm region of the spectra were analyzed with the assumption that the spectrum recorded at a given pH is a linear combination of those recorded for the neutral and anionic forms. Data analyses were based on the Henderson−Hasselbach equation:[31]

$$\epsilon(\lambda,\mathrm{pH}) = \frac{\epsilon_n(\lambda) + \epsilon_a(\lambda)10^{(\mathrm{p}K_a - \mathrm{pH})}}{1 + 10^{(\mathrm{p}K_a - \mathrm{pH})}}$$

where $\epsilon(\lambda, \mathrm{pH})$ is the spectrum recorded at a given pH, and $\epsilon_n(\lambda)$, $\epsilon_a(\lambda)$ are the spectra estimated for the neutral and anionic forms. The p$K_a$ values were determined using the Marquardt−Levenberg algorithm[27] implemented in the Gnuplot program.[28]

**Free Energy Calculation.** The differences between species with dissociation of the N(1)−H/N(3)−H or N(2)−H were estimated at the DF*T* theoretical level for compounds **1**−**7**. As reference for a non dissociable compound, the calculations were performed also for PMBT (**16**), m$^1$BT and m$^2$BT. The structures were built and initially optimized by *in vacuo* energy minimization with the Sybyl package, using the Tripos forcefield[32] and Amber atomic charges.[33] This was followed by *ab initio* analysis with the aid of the GAMESS 6.0 program.[34] The DFT calculations were performed with the B3LYP functional[35] using the 6-31G(d,p) basis set[36] in accord with the previous analysis of the BT systems.[14] For both tautometric and monoanionic forms, geometry optimizations were done using the PCM (polarizable continuum model) approach,[37] permitting computation of the electrostatic partition of solute interaction with the apparent surface charge distribution, the Claverie−Pierotti cavitation energy,[38] and dispersion and repulsion contributions to the solvation free energy.[35] The structures were initially preoptimized at the same theoretical level by *in vacuo* calculations. Calculations were performed independently for aqueous and DMSO solutions, using GAMESS standard solvent parametrization.

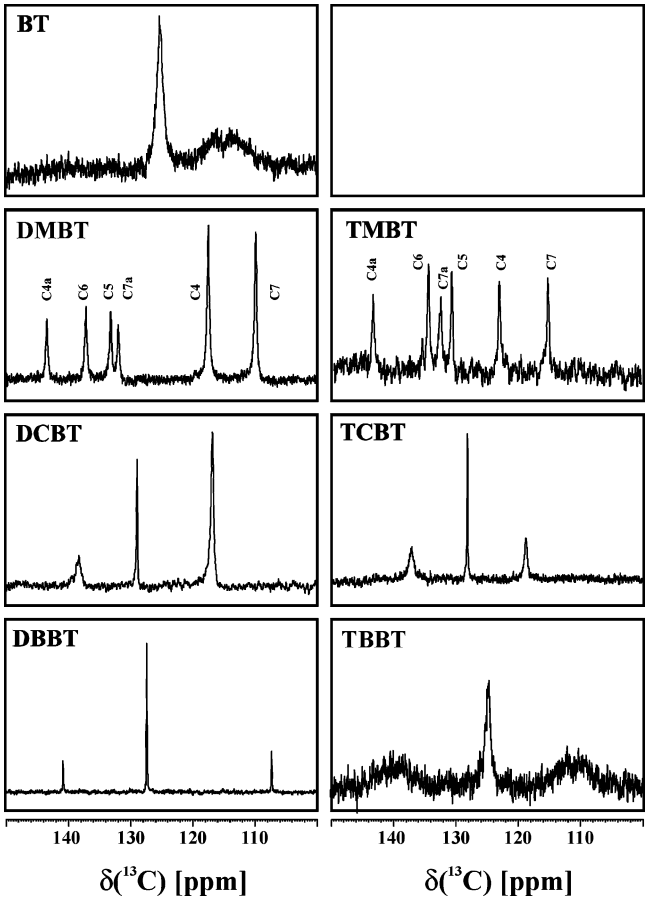


**Figure 1.** Aromatic regions of $^{13}$C spectra recorded for BT and its derivatives in DMSO solution.

**$^{13}$C NMR Shielding Calculations.** *Ab initio* calculations were performed using the gauge invariant atomic orbitals (GIAO) method implemented in the DALTON program.[39] The calculations were done using the HF/6-311G basis set, as the core orbitals mostly participates in the nuclear magnetic shielding. For all compounds the initial geometry was adopted from the final results of GAMESS calculations with the PCM model of the solvent.[37] Carbon shielding parameters were computed both for the vacuum state and by the use of the solvation model of a molecule in a spherical cavity in a dielectric medium.

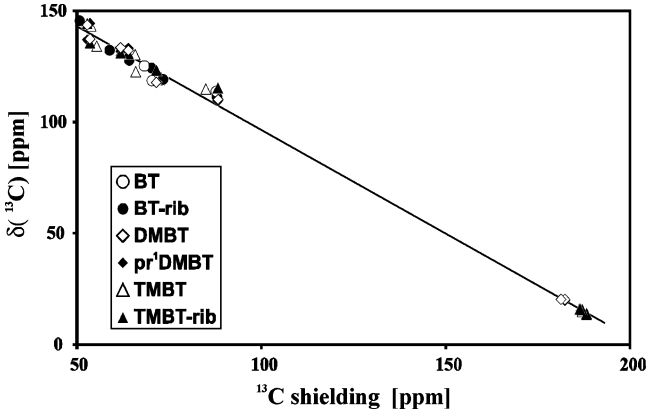


**Figure 2.** Comparison of experimentally determined $^{13}C$ chemical shifts with the GIAO-derived NMR shielding parameters for BT, DMBT, TMBT, and their N(1)-substituted derivatives. The solid line shows the correlation between theoretical and experimental values ($R^2$ = 0.995).

## III. Results and Discussion

**A. Resonance Assignments.** The $^{13}C$ NMR spectra of all compounds (see Scheme 2) were recorded in anhydrous DMSO, in order to minimize the proton exchange rate for those unsubstituted on the triazole ring (compounds **1**−**7**).

Whereas all spectra of N-substituted derivatives (**8**−**15**) (see Scheme 2) display narrow resonance lines (width ∼2 Hz), those of **1**−**7 (**Figure 1) are significantly broadened (Table 1), clearly due to existence of a dynamic prototropic equilibrium. Furthermore, for the latter, various patterns of resonance lines are observed, corresponding to a wide range of exchange rates, depending on the nature of the substituents on the benzene ring.

Assignments of individual $^{13}C$ resonances, based on quantum mechanical (GIAO) calculations of carbon nuclei shielding (Figure 2), using the HF/6-31G basis set, were in good accord with previously reported $^{13}C$ data for the parent benzotriazole (**1**)[40,41] and a series of N(1)-monosubstituted derivatives.[29,30] To further check the reliability of the basis set employed in the calculations, those for BT were also performed with more advanced basis sets, *viz.* HF/6-311G, HF/6-311++G and HF/6-311++G(d,p). The shielding parameters obtained at different theory levels were found to be highly correlated ($R^2 > 0.99$), and the energy difference between the two protomers remained identical within the range of 0.3 kcal/mol. The resonance assignments for one compound, the riboside of DCBT (**14**), were additionally confirmed by a $^{13}C-^{1}H$ HSQC experiment set up for 200 ms mixing time, optimal for 5 Hz heteronuclear coupling (cf. Table 1 for full assignment).

**B. NMR-Related Symmetry.** Reference spectra of the fixed tautomeric forms of TBBT, i.e., m[1]TBBT (**8**) and m[2]TBBT (**9**), and of DMBT, i.e., pr[1]DMBT (**10**) and pr[2]DMBT (**11**), exhibit qualitative differences in the resonance patterns, clearly related to molecular symmetry. The asymmetrical N(1)-alkyl derivatives, **8** and **10**, exhibit a pattern of six narrow lines (≈1.6 Hz line width) corresponding to six aromatic carbons (Figure 3). By contrast, the symmetrical N(2)-alkyl derivatives, m[2]TBBT (**9**) and pr[2]DMBT (**11**), both with kinetically averaged $C_{2v}$ symmetry (because of rapid rotation of the N(2) substituents), display in the low-field region of the spectra three degenerate resonance lines corresponding to three pairs of chemically equivalent aromatic carbon nuclei, C(4a)/C(7a), C(4)/C(7), and C(5)/C(6).

The aromatic regions of the $^{13}C$ spectra of DMBT (**4**) and TMBT (**7**) are also characterized by six distinct resonance lines, corresponding to the six chemically nonequivalent carbon nuclei in the benzene ring. However, in contrast to the spectra of the N(1)-alkyl congeners **8** and **10**, the resonance lines are much broader (50−55 Hz), pointing to existence of a relatively slow (on the $^{13}C$ NMR time scale) tautomeric exchange (Figure 1). The spectra of BT (**1**) and TBBT (**5**) demonstrate dramatic differences in the peak patterns. The C(5) and C(6) resonance lines, centered at ≈125 ppm, are now averaged, and the apparent resonance line width (≈150 Hz) points to a marked increase in the rate of the exchange process relative to DMBT and TMBT. The resonance lines located in the high-field region (≈114 ppm), assigned to C(4) and C(7), are extremely broad (≈1 kHz) and overlap. The resonance lines of C(4a) and C(7a) are either averaged to one extremely broad signal (TBBT), or absent due to coalescence (BT). The latter two spectra provide a unique insight into the exchange process. The time scale of the conformational exchange process is occasionally perfectly tuned with the spin properties of the nuclei involved in $^{13}C$ NMR

**TABLE 1: $^{13}C$ Resonance Assignments for BT Derivatives in DMSO and, in Some Instances, Following Addition of 1% (v/v) Water. Apparent Resonance Line Widths, in Hz, are in Brackets.**

| | $^{13}C$ chemical shifts [ppm] and resonance line widths [Hz] | | | | | |
|---|---|---|---|---|---|---|
| compound | δ(C(4a)) | δ(C(7a)) | δ(C(6)) | δ(C(5)) | δ(C(4)) | δ(C(7)) |
| BT (**1**) | *a* | | 125.2[b] (154) | | 118.6[c] | 113.8[c] |
| +$H_2O$[d] | *a* | | 125.5[b] | | 114.8[b] (382) | |
| DBBT (**2**) | 140.7[b] (17) | | 127.3[b] (11) | | 107.3[b] (13) | |
| + $H_2O$[d] | 140.6[b] (11) | | 127.7[b] (8) | | 107.2[b] (8) | |
| DCBT (**3**) | 138.5[b] (114) | | 129.2[b] (17) | | 117.1[b] (57) | |
| DMBT (**4**) | 143.3 (54) | 131.9 (48) | 137.0 (57) | 133.1 (55) | 117.5 (53) | 109.9 (54) |
| TBBT (**5**) | 139.4[b] (512) | | 124.8[b] (190) | | 114.3[c] | 109.5[c] |
| + $H_2O$[d] | 138.9[b] (57) | | 124.7[b] (13) | | 110.9[b] (54) | |
| TCBT (**6**) | 137.0[b] (115) | | 128.1[b] (17) | | 118.7[b] (70) | |
| +$H_2O$[d] | 136.9[b] (46) | | 128.1[b] (10) | | 118.6[b] (27) | |
| TMBT (**7**) | 143.1 (78) | 132.1 (82) | 134.1 (60) | 130.3 (53) | 122.6 (77) | 114.7 (72) |
| +$H_2O$[d] | 142.4 (334) | 132.8[e] (300) | 132.8[e] (280) | 130.5[e] (280) | 121.8 (315) | 114.9 (373) |
| m[1]TBBT (**8**) | 149.9 (2) | 137.5 (2) | 133.2 (2) | 128.5 (2) | 120.7 (2) | 112.3 (2) |
| m[2]TBBT (**9**) | 142.5[f] (2) | | 125.3[f] (2) | | 113.3[f] (2) | |
| pr[1]DMBT (**10**) | 144.3 (2) | 131.8 (2) | 136.9 (2) | 133.2 (2) | 117.9 (2) | 109.6 (2) |
| pr[2]DMBT (**11**) | 142.9[f] (2) | | 136.0[f] (2) | | 116.0[f] (2) | |
| BT-rib (**12**) | 145.5 (2) | 132.3 (2) | 127.7 (2) | 124.4 (2) | 119.3 (2) | 111.3 (2) |
| DBBT-rib (**13**) | 145.0 (2) | 132.1 (2) | 133.5 (2) | 128.5 (2) | 111.8 (2) | 102.0 (2) |
| DCBT-rib (**14**) | 144.5 (2) | 131.3 (2) | 131.0 (2) | 127.4 (2) | 120.6 (2) | 113.4 (2) |
| TMBT-rib (**15**) | 144.5 (2) | 131.0 (2) | 135.6 (2) | 130.9 (2) | 123.4 (2) | 115.2 (2) |

[a] Signal undetectable. [b] Two resonance lines averaged due to proton exchange. [c] Resonance position and line width deduced from the two-state chemical exchange model. [d] Addition of 1% (v/v) water to the sample dissolved in DMSO. [e] Overlapped resonances resolved by line-fitting. [f] The two nuclei are equivalent due to $C_{2v}$ symmetry.

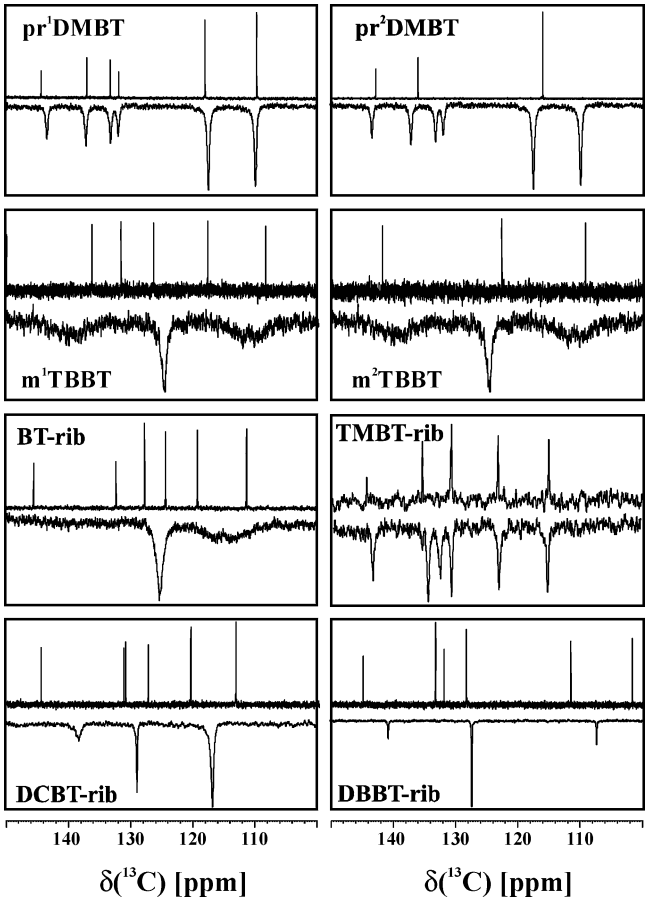


**Figure 3.** The $^{13}C$ spectra for pr$^1$DMBT, pr$^2$DMBT, m$^1$TBBT, and m$^2$TBBT in DMSO compared with those of their parent N-unsubstituted compounds (mirrored). The aromatic regions of the $^{13}C$ spectra of BT, TMBT, DCBT, and DBBT (mirrored) and those of the N(1)-ribose derivatives are also shown. The agreement between the resonance locations strongly points to predominance of the asymmetric prototropic form.

shielding. The very marked broadening of the C(4) and C(7) resonances is a consequence of the larger separation of the undisturbed resonance lines, so that the rate of the exchange process lies in the intermediate exchange regime. The spectral separation of the C(4a) and C(7a) resonances is much larger than for C(4) and C(7), hence the exchange process attains a coalescence boundary which, in the case of BT, leads to disappearance of the signals.

DCBT (**3**) and TCBT (**6**) each exhibits a set of three broad resonances, with line widths of ≈100, 50−60, and 16 Hz for C(4a)/C(7a), C(4)/C(7), and C(5)/C(6), respectively, hence following the tendencies observed for BT and TBBT (see above) and indicating that the effect of the protonation site, N(1) or the equivalent N(3), on the carbon nuclei decreases with the number of bonds separating a carbon atom from the proton acceptor, being most marked for the C(4a)/C(7a) nuclei proximal to the triazole ring, and weakest for the distal C(5)/C(6) nuclei. By contrast, the exchange process with DBBT (**2**) is sufficiently fast to locate all pairs of equivalent resonances in the fast exchange regime, characterized by three lines corresponding to the three degenerate resonance pairs, C(4a)/C(7a), C(4)/C(7), and C(5)/C(6), with line widths of 10 − 15 Hz (Figure 1).

**C. Effects of Addition of Water.** To examine whether the observed exchange process is directly linked with a tautomeric equilibrium involving inter- or intramolecular proton transfer, the spectra of BT (**1**), DBBT (**2**), TBBT (**5**), TCBT (**6**), and TMBT (**7**) were recorded following addition of a small amount

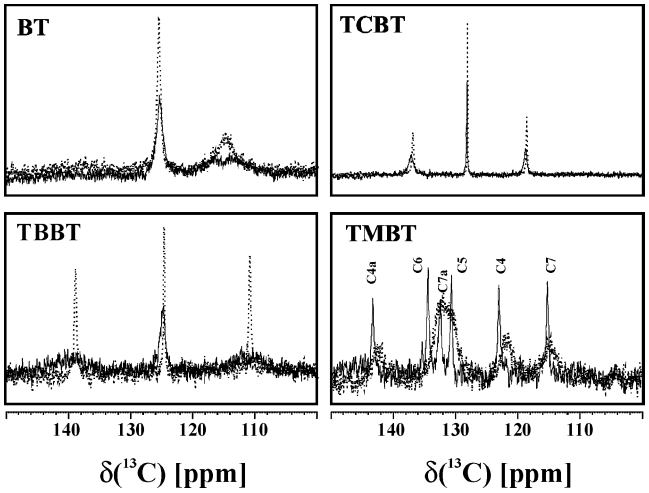


**Figure 4.** Effect of addition of 1% (v/v) of water to DMSO solution on $^{13}C$ spectra of BT, TCBT, TBBT, and TMBT (dotted line). The increase of exchange rate is resulting in narrowing the resonance lines of the compounds falling in medium exchange model in DMSO solution, while strong broadening is observed for the slowly exchanging TMBT.

of water (1% by volume) to the DMSO solutions. The resulting spectra are shown in Figure 4. With the exception of TMBT, there is efficient narrowing of all $^{13}C$ resonance lines, testifying to a significant increase in exchange rates. With TMBT (**7**), the increase of the exchange rate resulted in significant broadening of the resonance lines (280−350 Hz) relative to those recorded in anhydrous DMSO (50−55 Hz). Three of the signals, assigned to C(5), C(6), and C(7a), overlap. These increases in resonance line widths clearly demonstrate that the exchange process is also more rapid, but in this case falls in the intermediate exchange regime.

The foregoing establishes the existence of a prototropic equilibrium for the parent BT, as previously shown by others,[14,42] as well as for its derivatives **2**−**7** with an exchangeable proton on the triazole ring. Bearing in mind that addition of ∼1% water to the DMSO solutions significantly increases the rate of proton transfer, it follows that the exchange process in anhydrous DMSO involves mainly direct intramolecular proton transfer between the nitrogen atoms of the triazole ring. The $^{13}C$ line shapes in the spectra of BT, TBBT and TMBT, recorded additionally at 2-fold lower concentrations, were virtually unchanged, further supporting predominance of an intramolecular mechanism of proton transfer.

**D. Effects of an N-Substituent.** For the two compounds exhibiting significant differences in rates of prototropic exchange, DMBT (**4**) with a slow exchange rate, and TBBT (**5**) with a medium exchange rate, the N(1)- and N(2)-alkylated derivatives were then employed as references for identification of the sites of proton localization in the parent compounds.

Comparison of the $^{13}C$ spectra of DMBT (**4**), pr$^1$DMBT (**10**), and pr$^2$DMBT (**11**) revealed that the aromatic carbon chemical shifts for DMBT are almost identical (within a range of ∼0.4 ppm) with those of the N(1)-substituted derivative (Figure 3). Analogously, the $^{13}C$ spectrum of TMBT-rib (**15**) is close to that of the parent TMBT (**7**), with the largest perturbation observed for the C(7a) resonance, proximal to the ribosylated N(1). In the case of DCBT-rib, the mean values of the chemical shifts of the C(4a)/C(7a), C(5)/C(6), and C(4)/C(5) resonance pairs agree with the location of the $^{13}C$ signals for the parent DCBT, for which signal averaging due to prototropic exchange is observed.

Numerical analysis, based on the assumption that the observed NMR spectrum of DMBT is due to averaging of symmetrical and asymmetrical prototropic states, characterized by carbon chemical shifts close to the values measured for the corresponding derivatives **10** and **11**, respectively, leads to an estimate of the N(2)**—H** population, <5%. Taking into account that the observed resonance pattern for DMBT corresponds to a slow exchange regime, and that no peaks corresponding to the symmetrical form were detectable in the spectrum of DMBT, the population of the N(2) prototropic form is again estimated as <5%.

Analogously, in the case of TBBT (**5**), the aromatic region of the $^{13}$C spectrum may be approximately represented as the kinetically averaged spectra of N(1) and N(3) protonation states, supporting the dominance of the asymmetric prototropic form of the molecule. The location of the kinetically averaged resonance lines of the C(5) and C(6) nuclei in TBBT agrees with the average values of the C(5) and C(6) chemical shifts assigned in the $^{13}$C spectrum of m$^1$TBBT (**10**). The broad overlapping pairs of resonance lines of C(4a)/C(7a) and C(4)/C(7) are located symmetrically between the resonance lines of m$^1$TBBT (**10**). By contrast, the three degenerate lines in the aromatic region of the $^{13}$C spectrum of m$^2$TBBT (**11**) differ from the averaged positions of the corresponding pairs of resonances found for TBBT.

Additional evidence (albeit less quantitative) for dominance of the N(1)−H form of TBBT was provided by comparison of the UV spectrum of its neutral form in aqueous medium at pH 2 (p$K_a$ = 4.87) with those of its N(1)- and N(2)-alkyl congeners. The spectra of TBBT and pr$^1$TBBT resemble each other, and are markedly different from the spectrum of pr$^2$TBBT (data not shown). Numerical analysis proved that the population of H2 form of TBBT does not exceed 5%.

The more soluble N(1)-riboside derivatives were also employed to mimic the fixed N(1) prototropic form. In the case of TMBT-rib (**15**), the $^{13}$C NMR spectrum is closely similar to that of the parent TMBT (**7**). The resonance line of C(7a), proximal to the ribosylated N(1), exhibits the largest deviation from that found in TMBT (1.5 ppm), while the distal C(5) and C(6) are significantly less shifted (0.7 ppm).

With BT, the kinetically averaged resonance lines of C(5) and C(6) are in accord with the average values of the C(5) and C(6) chemical shifts assigned in the $^{13}$C spectrum of BT-rib (**12**), in the same manner as for TBBT and m$^1$TBBT. For the N(1)-ribose derivatives of DBBT, and DCBT, the locations of the averaged resonances for the parent compounds are in accord with the average values of the chemical shifts of the pairs of corresponding resonances, C(4a)/C(7a), C(4)/C(7), C(5)/C(6).

Summing up, it is clear that, for all compounds **1**−**7**, a prototropic equilibrium exists predominantly between the asymmetric N(1) and N(3), and the population of the N(2) protomer, if not totally absent, is low (<5%).

**E. *Ab initio* Modeling of Prototropic Equilibrium.** Calculations were performed for compounds **1**−**7** in both N(1) and N(2) prototropic forms, for their monoanionic states, and for the N(1)- and N(2)-methyl derivatives. For all molecules, the internal free energy was estimated for the two prototropic states and for the monoanionic form. Additionally, using the GIAO method, NMR shielding of carbon nuclei was estimated for BT, DMBT, TMDT and their N(1)- and N(2)- alkyl congeners.

For all compounds with exception of DMBT (4), in both DMSO and aqueous medium, the free energy of stabilization of the N(1) form exceeds 3 kcal/mol, virtually precluding existence of the symmetric, N(2) protomer, in accord with the NMR and UV spectral data. In the case of DMBT, the asymmetric form is also the more stable, but does not exclude a population of ∼10% of the symmetric form. For B*T* the results are consistent with the published NMR analysis of BT tautomerism, pointing to a population of the N(2) symmetric form below 5%.[42]

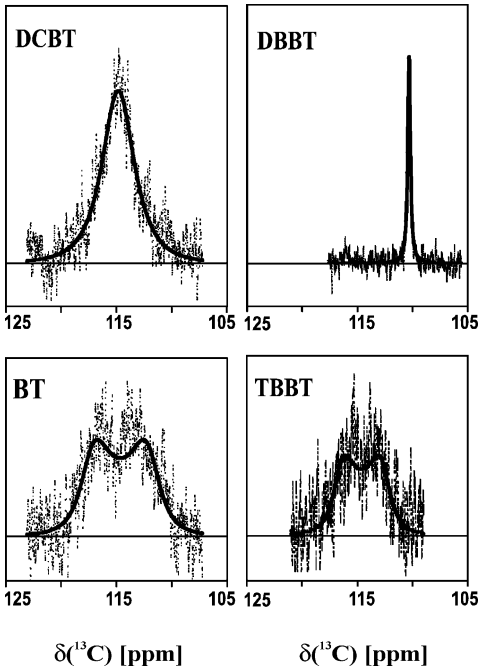


**Figure 5.** Analysis of the C(4)/C(7) resonance line shape based on the model of two equally populated states undergoing exchange. The solid line corresponds to the final model.

**F. Prototropic Exchange Rates.** Bearing in the mind the $^{13}$C chemical shift analysis of compounds **1**−**7**, especially the agreement with the spectra of the N(1) blocked analogs and the results of theoretical calculations showing significant free energy stabilization of the N(1)/N(3) tautomers, the line shapes of the observed C(4) and C(7) resonances were analyzed in terms of two equally populated interexchanging states. Both N(1) and N(3) protonated structures are identical from a chemical point of view, but not when related to a particular carbon nucleus. The local chemical structure of each significantly differs when the proton is located at N(1) or N(3). Thus, for each carbon nucleus the observed resonance signal arises from kinetically averaged states corresponding to frozen N(1) and N(3) proton localizations. When the exchange process is fast, the pair of resonance signals is averaged to one resonance line, and a pattern of three degenerate resonance lines is expected, as observed for DBBT, DCBT and TCBT. When the exchange process is absent, as in N(1)-substituted derivatives, or slow as in DMBT and TMBT, the pattern of six resonance lines corresponding to six aromatic carbon nuclei is observed. In such conditions the shape of the resonance line may be presented in the form:[43]

$$I(\omega) = \frac{K(\omega_2 - \omega_1)^2 I_o}{K^2(\omega - \omega_o)^2 + 4\pi^2(\omega - \omega_1)^2(\omega - \omega_2)^2}$$

where $I_0$ is a normalization factor, $\omega_1$, $\omega_2$ are the locations of a resonance line of a given nucleus in two states, $K$ is the exchange rate, and $\omega_0 = (\omega_2 + \omega_1)/2$.

The overall shape of the resonance line depends on the ratio $K/(\omega_2 - \omega_1)$. In the fast exchange regime, when $K \gg (\omega_2 - \omega_1)$, the resonance lines are averaged, and the higher the

**TABLE 2: Experimental $^{13}C$ Chemical Shifts and Calculated $^{13}C$ Nuclear Shielding (GIAO-Derived, Using the HF6-311G Basis Set) for BT Derivatives in DMSO**

| | nuclei | | | | | | $CH_3$ on | | | |
|---|---|---|---|---|---|---|---|---|---|---|
| compound | C(4A) | C(7A) | C(4) | C(7) | C(5) | C(6) | C(4) | C(5) | C(6) | C(7) |
| BT (**1**) | | | | | | | | | | |
| $\delta(^{13}C)$ | | | 118.6 | 113.8 | 125.2 | | | | | |
| shielding | 52.4 | 60.7 | 70.3 | 87.7 | 73.1 | 63.3 | | | | |
| | | | | | 68.2 | | | | | |
| DMBT (**4**) | | | | | | | | | | |
| $\delta(^{13}C)$ | 137.3 | 133.4 | 117.8 | 110.2 | 132.2 | 143.6 | | 20.3 | 20.3 | |
| shielding | 53.6 | 61.8 | 71.6 | 88.2 | 63.9 | 52.8 | | 182.3 | 181.3 | |
| TMBT (**7**) | | | | | | | | | | |
| $\delta(^{13}C)$ | 143.1 | 132.1 | 130.3 | 114.7 | 122.6 | 134.1 | 14.0 | 14.9 | 15.9 | 15.9 |
| shielding | 53.9 | 61.9 | 65.8 | 84.9 | 65.9 | 55.4 | 188.2 | 187.1 | 186.3 | 187.1 |
| DCBT (**3**) | | | | | | | | | | |
| $\delta(^{13}C)$ | 129.2 | | 117.1 | | 138.5 | | | | | |
| shielding | 53.8 | 62.2 | 69.0 | 85.5 | 61.3 | 51.4 | | | | |
| | 58.0 | | 77.3 | | 56.3 | | | | | |
| TCBT (**6**) | | | | | | | | | | |
| $\delta(^{13}C)$ | 128.1 | | 118.7 | | 137.0 | | | | | |
| shielding | 56.4 | 63.1 | 58.7 | 74.8 | 61.7 | 52.9 | | | | |
| | 59.7 | | 66.7 | | 57.3 | | | | | |

**TABLE 3: Calculated, for Compounds 1−7, Free Energy of Stabilization of the N(1)−H Form vs the N(2)−H, $\Delta G(2,1)$, Relative Free Energy Changes on Dissociation, $\Delta\Delta G(a,1)$, Experimental (NMR-Derived) Rates, $k_{exchange}$, of N(1) ↔ N(3) Proton Transfer in Anhydrous DMSO, and Experimental p$K_a$ Values in Aqueous Medium and in 50% Aqueous Ethanol**

| compound | | $\Delta G(2,1)$ [kcal/mol] | | $\Delta\Delta G(a,1)$ [kcal/mol] | | $k_{exchange}$ [$s^{-1}$] | p$K_a$ value in | |
|---|---|---|---|---|---|---|---|---|
| | | $H_2O$ | DMSO | $H_2O$ | DMSO | DMSO | $H_2O$ | $H_2O$/ethanol[45,a] |
| TCBT | (**6**) | 3.57 | 3.44 | 0.00 | 0.00 | 3600 ± 950 | 4.57, 4.52[44] | 5.10 |
| TBBT | (**5**) | 3.69 | 3.60 | 2.03 | 2.01 | 2500 ± 300 | 4.87−5[21] | |
| BT | (**1**) | 4.37 | 4.31 | 6.00 | 6.10 | 2000 ± 600 | 8.56, 8.67,[44] 8.38[46] | |
| DCBT | (**3**) | 4.37 | 4.30 | 6.30 | 6.43 | 1100 ± 500 | 7.00 | 6.85 |
| DBBT | (**2**) | 4.38 | 4.31 | 7.52 | 7.55 | 1500 ± 900 | 5.68 | |
| TMBT | (**7**) | 3.28 | 3.12 | 9.01 | 8.92 | 346 ± 20 | 8.85 | |
| DMBT | (**4**) | 0.92 | 0.90 | 17.35 | 17.54 | 322 ± 10 | 9.32 | 9.98 |

[a] Numbers in superscript are references.

exchange rate, the narrower is the line observed. With a slow exchange regime, $K \ll (\omega_2 - \omega_1)$, the two resonance lines corresponding to the two separate nuclear spins are visible, and the slower the exchange rate, the narrower the resonance lines. In the intermediate exchange regime, $K \sim (\omega_2 - \omega_1)$, a single extremely broad resonance signal is observed. According to the theoretical $K(\Delta\omega)$ relationship, DMBT and TMBT, which exhibit patterns of six resonance lines in the downfield region of the spectra, experience slow prototropic exchange, with a rate significantly lower than the resonance separation. In the case of DBBT, DCBT, and TCBT, the prototropic equilibrium falls in the fast exchange regime, while the spectra of BT and TBBT are characteristic for spin systems in the medium exchange regime.

The spectral regions corresponding to C(4) and C(7) were then analyzed using the proposed model of exchange. Values of chemical shifts were first adopted from the N(1)-substituted derivatives, and initially only $I_0$ and $K$ values were optimized, followed by unconstrained optimization of all parameters. When applied to DMBT and TMBT, this gave precise estimates of exchange rates, since both (C(4) and C(7)) were well separated. With BT and TBBT, experiencing the intermediate exchange regime, analysis also leads to estimates of exchange rates; but, due to the strong correlation of the model parameters (e.g., K with $\omega_2 - \omega_1$), the K values are much more biased than those estimated for DMBT and TMBT. With DCBT and TCBT, exhibiting a signal averaging pattern characteristic of the fast exchange regime, the exchange rates were estimated with an error ∼50%.

For all analyzed compounds, the model of two equally populated interexchanging states satisfactorily reproduces the experimentally determined $^{13}C$ NMR spectra, presented in Figure 5 for BT, DCBT, DBBT, and TBBT.

**G. Anionic form of BT as the Rate-Limiting State.** The experimentally observed proton exchange, attributed to the N(1)/N(3) protonation equilibrium, is based on a comparison of the $^{13}C$ spectra of the seven compounds with an exchangeable proton on a triazole ring nitrogen with their N(1)/N(2)-alkyl or N(1)-riboside derivatives. The proton exchange rates, estimated on the basis of a model of two equally populated states, are presented in Table 2. In anhydrous DMSO, the possible presence of only an infinitesimal amount of $H_2O$ precludes participation of water molecules in proton transfer, and the exchange process must be driven by either intra- or intermolecular proton transfer between N(1) and N(3). Since the $^{13}C$ spectra of BT, TBBT and TMBT were found virtually unchanged over a 2-fold concentration range, intramolecular proton transfer may be regarded as predominant. Thus, the anionic forms of **1**−**7** are the candidates for the rate-limiting transition state on the pathway of intramolecular proton transfer. The N(2)−H form of benzotriazole, with a population <5%, become the putative trap on the pathway of proton-transfer.

Consequently, the height of the barrier on the N(1) ↔ N(3) proton-transfer pathway roughly corresponds to the free energy change upon proton dissociation, $\Delta\Delta G$(N-A), estimated with the aid of QM calculations. Substitution of four halogen atoms in the benzene ring (TBBT, TCBT) significantly decreases the free energy of proton dissociation, as compared with BT, DBBT, and DCBT. On the other hand, substitution of an electron-donating methyl group in BT increases the dissociation barrier, as both calculated and observed for TMBT and DMBT. Furthermore, the effect of substituents on the benzene ring is not additive, e.g., the free energy of proton dissociation for DMBT was found significantly higher than for TMBT.

The QM-derived barrier heights for the N(1) ↔ N(3) proton-transfer processes are collected in Table **3**. The calculated

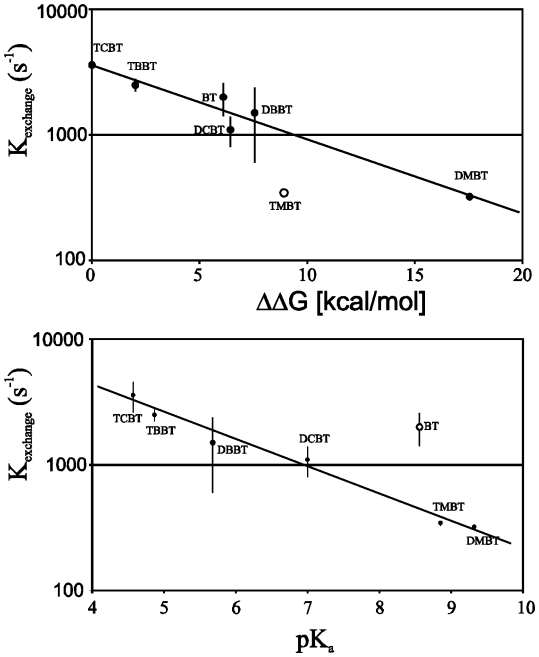


**Figure 6.** Experimentally measured rates of chemical exchange corresponding to the N(1)/N(3) prototropic equilibrium ($K_{exchange}$), determined for BT and its derivatives in DMSO, shown as a function of (upper) the QM-derived barrier height, and (lower) the experimental p$K_a$ values in aqueous medium.

change of the free energy for proton dissociation is a measure of the p$K_a$ for this process. And, in fact, experimental p$K_a$ values for compounds **1**−**7**, determined in aqueous medium, correlate well with the free energy changes for dissociation estimated from QM calculations. The theoretically estimated values of the free energy changes upon proton dissociation in DMSO are also correlated with the experimentally observed proton-transfer rates (Figure 6), supporting the proposal that the anionic form is the rate-limiting transition state. Furthermore, the p$K_a$ values determined by spectrophotometric titration are correlated with the NMR-derived chemical exchange kinetics (Figure 6), again pointing to the anionic form as the rate-limiting state. The results of QM calculations generally agree with a reported analysis of the tautomerism of benzotriazole.[14]

## IV. Summary

The following model for the tautomeric equilibrium in DMSO solution of BT and its derivatives may be proposed. For all molecules carrying an exchangeable proton, the asymmetric N(1)−H or N(3)−H states are preferentially populated. Occupancy of the symmetric, N(2)−H state is negligible ($<10^{-2}$). The N(1)−H and N(3)−H protomers are in dynamic equilibrium via intramolecular proton transfer, with an exchange rate of $10^2$−$10^3$ $s^{-1}$, and the rate-limiting transition state may be attributed to the anionic form. The magnitude of the rate depends on the nature of the substituents on the benzene ring. The QM-estimated free energy differences between the anionic and neutral forms correlates with NMR-derived rates of prototropic exchange. When a small amount of water is added to the DMSO solution, the water molecules mediate in the proton-transfer process, significantly increasing the rate of tautomeric/prototropic exchange. In aqueous medium the exchange rate is significantly higher, and all the spectra reflect the dynamically averaged $C_{2v}$ symmetry of the parent molecules. As may be concluded from the NMR data,[14] the population of N(2)−H is decreased upon substitution of electron-attracting groups on the benzene ring.

**Acknowledgment.** The presented work was supported in part by EC Grant FP5RTD No. QLRT-2001-01079 and national grant PBZ-MIN-014/P05/2004. The authors thank Grzegorz Bakalarski from Interdisciplinary Centre for Mathematical and Computational Modeling, Warszawa, Poland, for the help in setting up some QM calculations.

**Supporting Information Available:** Figure showing a comparison of the 3D structures of the α-subunit of *Zea mays* CK2 kinase and the complex with *Homo sapiens* phospho-CDK2/cyclin A. This material is available free of charge via the Internet at http://pubs.acs.org.

## References and Notes

(1) Elguero, J.; Katritzky, A. R.; Dfnisko, O. V. *Adv. Hetero. Chem.* **2000**, *76*, 157−323.
(2) Borowski, P.; Deinert, J.; Schalinski, S.; Bretner, M.; Ginalski, K.; Kulikowski, T.; Shugar, D. *Eur. J. Biochem.* **2003**, *270*, 1645−1653.
(3) Sarno, S.; Ruzzene, M.; Frascella, P.; Pagano, M. A.; Meggio, F.; Ambon, A.; Mazzorana, M.; Di, Maira, G.; Lucchini, V.; Pinna, L. A. *Mol. Cell. Biochem.* **2005**, *274*, 69−76.
(4) Catalan, J.; Perez, P.; Elguero, J. *J. Org. Chem.* **1993**, *58*, 5276−5277.
(5) Tomas, F.; Catalan, J.; Perez, P.; Elguero, J. *J. Org. Chem.* **1994**, *59*, 2799−2802.
(6) Roth, W.; Spangenberg, D.; Janzen, Ch.; Westphal, A.; Schmitt. M. *Chem. Phys.* **1999**, *248*, 17−25.
(7) Ueno, L. T.; Ribero, R. O.; Rocha, M. S.; Suarez-Iha, M. E. V.; Iha, K.; Machado, F. B. C. *J. Mol. Struct. THEOCHEM* **2003**, *207*, 664−665.
(8) Escande, A.; Galigné, J. L.; Lapasset, J. *Acta Crystallogr. B* **1974**, *30*, 1490−1495.
(9) Fischer, G.; Cao, X. L.; Purchase, R. L. *Chem. Phys. Lett.* **1996**, *262*, 689−698.
(10) Palmer, M. H.; Kurshid, M. M. P.; Rayner, T. J.; Smith, J. A. S. *Chem. Phys.* **1994**, *182*, 27−37.
(11) Bigotto, A.; Pandey, A.; Zerbo, C. *Spectrosc. Lett.* **1996**, *29*, 511−522.
(12) Jacoby, Ch.; Roth, W.; Schmitt. M. *Appl. Phys. B: Laser Opt.* **2000**, *71*, 643−649.
(13) Fagel, J. E.; Ewing, G. W. *J. Am. Chem. Soc*. **1951**, *73*, 4360−4362.
(14) Jagerovic, N.; Jimeno, M. L.; Alkorta, I.; Elguero, J.; Claramunt, R. M. *Tetrahedron* **2002**, *58*, 9089−9094.
(15) Gaemers, S.; Elsevier, C. *J. Magn. Reson. Chem.* **2000**, *38*, 650−654.
(16) Lunazzi, L.; Parisi, F .; Macciantelli, D. *J. Chem. Soc., Perkin Trans. II* **1984**, 1025−1028.
(17) Nesmeyanov, A. N.; Babin, V. N.; Fedorov, L. A.; Rybinskaya, M. I.; Fedin, E. I. *Tetrahedron* **1969**, *25*, 4667−4670.
(18) Battistutta, R.; De Moliner, E.; Sarno, S.; Zanotti, G.; Pinna, L. A. *Protein Sci*. **2001**, *10*, 2200−2206.
(19) De Moliner, E.; Brown, N. R.; Johnson, L. N. *Eur. J. Biochem.* **2003**, *270*, 3174−3181.
(20) Dobrowolska, G.; Muszynska, G.; Shugar, D. *Biochim. Biophys. Acta* **1991**, *1080*, 221−226.
(21) Zien, P.; Duncan, J. S.; Skierski, J.; Bretner, M.; Litchfield, D. W.; Shugar, D. *Biochim. Biophys. Acta* **2005**, *1754*, 271−280.
(22) Zien, P.; Bretner, M.; Zastapilo, K.; Szyszka, R.; Shugar, D. *Biochem. Biophys. Res. Commun.* **2003**, *306*, 129−133.
(23) Bretner, M.; Baier, A.; Kopanska, K.; Najda, A.; Schoof, A.; Reinholz, M.; Lipniacki, A.; Piasek, A.; Kulikowski, T.; Borowski, P. *Antivir Chem. Chemother*. **2005**, *16*, 315−326.
(24) Kopanska, K.; Najda, A.; Zebrowska, J.; Chomicz, L.; Piekarczyk, J.; Myjak, P.; Bretner, M. *Bioorg. Med. Chem.* **2004**, *12*, 2617−2624.
(25) Borowski, P.; Deinert, J.; Schalinski, S.; Bretner, M.; Ginalski, K.; Kulikowski, T.; Shugar, D. *Eur. J. Biochem.* **2003**, *270*, 1645−1653.
(26) Cobas, C.; Cruces, J.; Sardina, F. J. MestRe-C 2.3a, Magnetic Resonance Companion NMR Data Processing Program. Departamento de Química Orgánica, Facultad de Química, Universidad de Santiago de Compostela, 1706 Santiago de Compostela Spain.
(27) Marquardt, D. W. *J. Soc. Ind. Appl. Math.* **1963**, *11*, 431−441.
(28) Williams, T.; Kelley, C. Gnuplot, Version 4.0. http://www.ucc.ie/gnuplot, **2004.**
(29) Katritzky, A. R.; Fali, C. N.; Oniciu, D. C. *Tetrahedron* **1995**, *51*, 1069−1076.
(30) Katritzky, A. R.; Toader, D.; Jiang, J. *J. Org. Prep. Proc. Int.* **1995**, *27*, 179−184.

(31) Krekel, F.; Samland, A. K.; Macheroux, P.; Amrhein, N.; Evans, J. N. *Biochemistry* **2000**, *39*, 12671−12677.
(32) Clark, M.; Cramer, R. D.; Van Opdenbosh, N. *J. Comput. Chem.* **1989**, *20*, 982−1012.
(33) Weiner, J. S.; Kollman, P. A.; Case, D. A.; Singh, U. C.; Ghio, C.; Alagona, G.; Profeta, S.; Weiner. P. *J. Am. Chem. Soc.* **1984**, *106*, 765−784.
(34) Schmidt, M. W.; Baldridge, K. K.; Boatz, J. A.; Elbert, S. T.; Gordon, M. S.; Jensen, J. J.; Koseki, S.; Matsunaga, N.; Nguyen, K. A.; Su, S.; Windus, T. L.; Dupuis, M.; Montgomery, J. A. *J. Comput. Chem.* **1993**, *14*, 1347−1363.
(35) Hertwig, R. H.; Koch, W. *Chem. Phys. Lett.* **1997**, *268*, 345−351.
(36) Francl, M. M.; Pietro, W. J.; Hehre, W. J.; Binkley, J. S.; Gordon, M. S.; DeFrees, D. J.; Pople, J. A. *J. Chem. Phys.* **1982**, *77*, 3654−3665.
(37) Cammi, R.; Tomasi, J. *J. Comput. Chem.* **1995**, *16*, 1449−1458.
(38) Langlet, J.; Claverie, P.; Caillet, J.; Pullman, A. *J. Phys. Chem.* **1988**, *92*, 1617−1631.
(39) Helgaker, T.; Jensen, H. J. A.; Joergensen, P.; Olsen, J.; Ruud, K.; Aagren, H.; Auer, A. A.; Bak, K. L.; Bakken, V.; Christiansen, O.; Coriani, S.; Dahle, P.; Dalskov, E. K.; Enevoldsen, T.; Fernandez, B.; Haettig, C.; Hald, K.; Halkier, A.; Heiberg, H.; Hettema, H.; Jonsson, D.; Kirpekar, S.; Kobayashi, R.; Koch, H.; Mikkelsen, K. V.; Norman, P.; Packer, M. J.; Pedersen, T. B.; Ruden, T. A.; Sanchez, A. Saue, T.; Sauer, S. P. A.; Schimmelpfennig, B.; Sylvester-Hvid, K. O.; Taylor, P. R.; Vahtras, O. Dalton, a molecular electronic structure program, Release 1.2, 2001.
(40) Schilf, W.; Stefaniak, L.; Witanowski, M.; Webb, G. A. *Bull. Pol. Acad. Sci., Chem.* **1985**, *33*, 437.
(41) Wiench, J. W.; Stefaniak, L.; Barszczewicz, A.; Webb, G. A. *J. Mol. Struct.* **1994**, *327*, 321−326.
(42) Wiench, J. W.; Koprowski, M.; Stefaniak, L.; Webb, G. A. *Pol. J. Chem.* **2002**, *76*, 525−536.
(43) Gunther, H. *NMR Spectroscopy: An Introduction*; John Wiley & Sons: Chichester, U.K., 1980.
(44) Wiley, Rh.; Hussgn, K. H.; Moffat, J. *J. Am. Chem. Soc.* **1955**, *77*, 5105−5108.
(45) Aten, W. C.; Buchel, K. H. *Z. Naturforsch. B* **1970**, *25*, 961−965.
(46) Hansen, L. D.; West, B. D.; Baca, E. J.; Blank, C. L. *J. Am. Chem. Soc.* **1968**, *90*, 6588−6592.